Journal of Engineering Mechanics, Vol. 136, No. 5, May 1, 2010, 641–652

Complex frequencies in elastodynamics, with application to the Damping-Solvent Extraction method

by
Eduardo Kausel[1]

Abstract

This paper addresses the use of complex frequencies in problems of wave propagation and structural vibrations. The most common form of application is as artificial damping that is extracted after the response in the time domain has been obtained. Then again a rather unorthodox application is in the simulation of systems of infinite spatial extent by means of finite systems modeled with discrete methods such as finite elements, a task that can be accomplished even when no transmitting or absorbing boundaries are used. This latter application of complex frequencies, which goes by the name *Damping-Solvent Extraction* method or its acronym DSE, is assessed herein by means of *exact* solutions to canonical problems that are used to establish the conditions that must be met by the finite models to work as intended, especially the size of the models, the magnitude of the imaginary component of frequency, and the limitations of the method.

Key words: Damping-solvent extraction method; exponential window method; absorbing boundaries; soil-structure interaction; correspondence principle; integral transforms; wave propagation; structural dynamics; geophysics; mechanical vibration.

Introduction

Inasmuch as frequency response functions exhibit sharp peaks at the resonant frequencies of lightly damped (or undamped) mechanical and structural systems, and these make numerical evaluation of inverse Fourier transforms difficult, complex frequencies were introduced by Phinney (1965) as a means to artificially dampen the frequency response function of seismograms in layered media while allowing this damping to be extracted later on, i.e. to be removed after the transformation was completed. This technique has since been used widely and very successfully in seismology. Kausel and Roësset (1992) and Hall and Beck (1993) applied a similar technique to obtain the dynamic response of *undamped* structural systems —both discrete and continuous— and showed that one can obtain virtually exact results in the time domain. The method avoids any "wraparound" in the response, and thus obviates the need for "trailing zeroes" or a "quiet zone" in the frequency response functions. Later on, Wolf and Song (1994) applied this concept in a rather unorthodox way, namely to obtain impedances for infinite media by means of finite models, a technique that they referred to as the *damping-solvent extraction* method (DSE). In a nutshell, this technique consists in adding artificial damping to a numerical model with finite elements so as to attenuate the waves that radiate out and reflect at the outer boundaries of the model. Hence, such waves never return to the region where the impedances are evaluated, which means that these impedances "never know" that the model stops somewhere. Hence, after the damping is *extracted*, what remains in the neighborhood of the sources is the undamped dynamic stiffness of an *infinite* region. In a sense this strategy achieves the same effect as an absorbing boundary, even when one is not explicitly used. However, the method was

[1] Professor of Civil and Environmental Engineering, Massachusetts Institute of Technology, Cambridge, MA 02139

demonstrated only by means of numerical experiments that did not provide any profound insights on how one chooses the magnitude of the artificial damping vis-à-vis the size and material properties of the model. In addition, the original theoretical formulation of the DSE was lacking in rigor, and the empirical proof of concept resorted to models containing numerous confounding effects, such as discretization errors, elastic foundations, absorbing boundaries, or material damping, all of which made general assessments and predictions difficult. This situation led Basu and Chopra (2002) to carry out a lengthy assessment of this method in which they attempted to pin down some of the missing characteristics, but they attained only mixed results that still left many unanswered questions. For this reason, we take up this subject here again and explore the use of complex frequencies in the context of the DSE by means of *exact*, yet simple canonical models that provide greater transparency into the effects of the various parameters.

We begin by showing the equivalence of complex frequencies to a form of damping and how this damping can be extracted, then proceed summarizing the *correspondence principle* on which the DSE is based, and go on to apply complex frequencies to five canonical models that are free from confounding effects. Finally, we demonstrate the effectiveness of the DSE method for a broad range of frequencies.

Complex frequencies as a form of damping

Consider an isotropic, locally homogenous viscoelastic system subjected to dynamic sources somewhere, for example, a layered soil. To keep the formulation simple, we consider here only a plane, two-dimensional system with mass-proportional viscoelastic damping, but this could readily be generalized to three dimensions and to a medium that also adds material damping. At some point in the medium without body forces, and after division by the mass density ρ, the dynamic equilibrium equation for mass-proportional damping is of the form

$$\begin{Bmatrix} C_P^2 & 0 \\ 0 & C_S^2 \end{Bmatrix} \frac{\partial^2 \mathbf{u}}{\partial x^2} + \left(C_P^2 - C_S^2\right) \begin{Bmatrix} 0 & 1 \\ 1 & 0 \end{Bmatrix} \frac{\partial^2 \mathbf{u}}{\partial x \partial y} + \begin{Bmatrix} C_S^2 & 0 \\ 0 & C_P^2 \end{Bmatrix} \frac{\partial^2 \mathbf{u}}{\partial y^2} = \frac{\partial^2 \mathbf{u}}{\partial t^2} + 2\eta \frac{\partial \mathbf{u}}{\partial t} + \eta^2 \mathbf{u} \qquad (1)$$

in which $\mathbf{u} = \mathbf{u}(\mathbf{x}, t)$ is the displacement vector, C_P, C_S are the local dilatational (P) and shear (S) wave velocities, and η is a parameter with dimension of frequency. Of the three terms on the right hand side, the first term is the acceleration, the second is mass-proportional viscous damping, and the third is equivalent to an elastic foundation. If $\eta = 0$, the system is undamped. While C_P, C_S, ρ may change from one region to another (e.g. layers), we take η to be constant throughout the entire system. This implies that the magnitude of the distributed damper that connects any point $\mathbf{x}$ to the fixed inertial reference frame is proportional to the mass density, i.e. $c = \rho\eta$, hence the designation "mass-proportional". Assuming that we formulate the solution by superposition of plane waves in all directions, and that these are of the form $\mathbf{u} = \mathbf{a} \exp \mathrm{i}(\omega t - \mathbf{k} \cdot \mathbf{x})$, we obtain after carrying out differentiations and collecting terms

$$\begin{Bmatrix} (\omega - \mathrm{i}\eta)^2 - k_x^2 C_P^2 - k_y^2 C_S^2 & \left(C_P^2 - C_S^2\right) k_x k_y \\ \left(C_P^2 - C_S^2\right) k_x k_y & (\omega - \mathrm{i}\eta)^2 - k_x^2 C_S^2 - k_y^2 C_P^2 \end{Bmatrix} \mathbf{a} = \mathbf{0} \qquad (2)$$

For a fixed horizontal wavenumber k_x and *complex* frequency $\varpi = \omega - i\eta$, this is an eigenvalue problem in the vertical wavenumber k_y with eigenvector $\mathbf{a}$ giving the polarization of the wave, which leads to the dispersion equations for P and S waves

$$k_x^2 + k_y^2 = \left(\frac{\varpi}{C_P} \right)^2 \qquad \text{for P waves} \tag{3a}$$

$$k_x^2 + k_y^2 = \left(\frac{\varpi}{C_S} \right)^2 \qquad \text{for S waves} \tag{3b}$$

Other than the change from real to complex frequency, equations 3a, 3b are *identical* to the dispersion equations for an *undamped* medium, and because η is constant throughout the system, ϖ does not depend on any of the other material characteristics of the medium. Hence, the displacement and stress continuity equations at material transitions remain identical to those of the undamped medium for any value of η, which means that the intrinsic solution for the problem remains the same as the elastic one, albeit with a complex frequency.

Assume next that the frequency response function at some arbitrary point $\mathbf{x}$ in the damped system is obtained by numerical means, and that the response in time is recovered from the inverse Fourier transform

$$\mathbf{u}(\mathbf{x}, t, \eta) = \tfrac{1}{2\pi} \int_{-\infty}^{+\infty} \mathbf{u}(\mathbf{x}, \omega, \eta) e^{i\omega t} d\omega \tag{4}$$

which for non-negative time $t \geq 0$ can be evaluated by contour integration in the upper complex half-plane

$$\mathbf{u}(\mathbf{x}, t, \eta) = \tfrac{1}{2\pi} \oint \mathbf{u}(\mathbf{x}, z, \eta) e^{\mathrm{i}zt} dz \tag{5}$$

Now, from considerations of causality, we know that the lower complex half-plane $\operatorname{Im} z < 0$ cannot contain any poles, because if it did, the system would begin responding at negative times to any causal source. Hence, when modeling a source and carrying out contour integrations from frequency into time, it is permissible to close the contour along a horizontal frequency axis that is shifted *downward* in the complex plane by an amount $i\eta$, and set

$$\exp i\omega t = \exp i(\varpi + i\eta)t = \exp i\varpi t \, \exp(-\eta t), \qquad d\varpi = d\omega \tag{6}$$

With this shift, we see that we are able to reproduce *exactly* the Fourier integral for a fully elastic medium, except that there is now an additional exponential factor $\exp(-\eta t)$ that attenuates the response. Since η is not a function of space, this implies that the term $\exp(-\eta t)$ can be factored out of the integral, so the response in space-time will be identical to that of the elastic medium except for an exponential decay that modulates the response. We are then led to the following conclusions:

- The response of the system with mass-proportional, artificial damping of the form given by equation 1 is *identical* to the response of the fully elastic system, except that it is attenuated by a multiplicative *decaying exponential window*, $\exp(-\eta t)$.
- Any numerical formulation based on the use of FFT's which avoids resonances and waviness in the kernels of the transfer functions by working with complex frequencies with a *constant, negative* imaginary part is equivalent to adding a form of mass-proportional, viscous damping. Furthermore, this damping can be "extracted" *after* the time signatures have been obtained. Indeed, it suffices to multiply the numerically obtained, damped response functions by a *rising exponential window* $\exp(\eta t)$. However, to prevent gross errors towards the end of the time window, η cannot be chosen arbitrarily large, but cannot exceed the frequency step used in the FFT, i.e. $\eta \le \Delta\omega$. Further details can be found in Kausel and Roësset, 1992 and in Hall and Beck (1993).

Correspondence Principle

A fundamental theorem due to Biot, the so-called correspondence principle, states that if one adds damping to an undamped system and the viscosity has the same spatial variation as the material parameters, then the damped response can be obtained directly from the undamped response simply by replacing the real-valued elastic moduli with complex moduli in the formulas for the response. For instance, in the case of viscous damping, the real shear modulus must be replaced by a complex modulus according to the rule $G^* = G\left(1 + 2\mathrm{i}\xi\,\omega/\omega_{ref}\right)$, where ξ is a fraction of critical damping that does not depend on the spatial coordinates, ω is the driving frequency, and ω_{ref} is a reference frequency used to calibrate ξ (i.e. to define its meaning). However, in most practical problems, and especially those that rely on numerical solutions, the frequency response functions $F(\omega)$ are known only numerically, and not in terms of a formula. Examples of such frequency-response functions are the impedance functions of a rigid foundation underlain by an elastic medium that are obtained via finite elements. Thus, one is not able, after these functions have been computed, to plug in complex moduli into the tables of numbers or into the frequency-response plots. However, it seems natural to think that one can still accomplish this objective without repeating the numerical calculations with complex moduli by viewing damping as a perturbation whose effect can be estimated via Taylor series. The success of this strategy hinges in part on the analyticity of the frequency-response functions.

The reader may recall that for a function of complex variable $f(z) = u(x,y) + \mathrm{i}\,v(x,y)$ with $z = x + \mathrm{i}\,y$, if the function is *analytic* in some region, then it must satisfy the Cauchy-Riemann conditions $u_{,x} = v_{,y}$, $u_{,y} = -v_{,x}$, with commas denoting partial derivatives. These conditions imply that at points where the function is analytic, the derivative satisfies $f'(z) = f_{,z} = f_{,x} = f_{,\mathrm{i}y}$, so when the function is analytic at some point z, the derivative is the same in all directions. Also, the function has derivatives of all orders in that region, and it can be expanded in Taylor series that converges within the circle with center at z that extends to the nearest singular point.

In principle, when a well-behaved, linearly viscoelastic and arbitrarily damped mechanical system of either finite or infinite extent is subjected to dynamic sources somewhere and the

response at any arbitrary point in the system is sought in the frequency domain, one is led to complex valued frequency response functions that, except for of the singularities at the location of the system poles, are analytical functions of frequency. Such functions are assured to be invertible into the time domain, that is, to have a Fourier transform that can be evaluated by contour integration in terms of the residues at the poles. In the case of systems of infinite extent, the contour integrals might also involve so-called branch integrals that add the contribution of inhomogeneous waves, but this is of no concern to us here. That the frequency-response functions must be Fourier invertible can also be argued on physical grounds: for any arbitrary elastic system, the signatures in time must exist, and they must obey causality. The analyticity of these functions guarantees that one can expand the frequency response functions $F(\omega)$ in Taylor series, to extrapolate the response from one level of damping to some other *nearby* level (i.e. small changes in damping). In those cases the derivatives with respect to frequency can be estimated numerically by differentiation, or even obtained with modest additional computational effort directly and simultaneously with the response, as was done by Basu and Chopra (2002).

In contrast, inverses of flexibility functions $K(\omega) = F^{-1}(\omega)$, namely the stiffness or impedance functions, do not necessarily possess Fourier transforms, because they generally fail the requisite Dirichlet conditions for such transforms to exist. In addition, these stiffness functions have poles at the complex *zeros* of the flexibility functions, and since these need not be located in the upper complex frequency half-plane, the stiffness functions need not, in general, obey causality. It is then rather remarkable that stiffness functions should turn out to be far more tolerant of large —or even enormous— perturbations in damping than the flexibility functions. As will be seen, the DSE method works very well even with superlatively large imaginary components of frequency that cannot be regarded as simple "perturbations", which is not the case with flexibility functions. For the latter, the Taylor series extrapolation procedure breaks down miserably unless the change in damping is small, a precondition that would nullify the effectiveness of the DSE. The reason may well be as follows.

Consider either a discrete or continuous system and focus attention on some arbitrary frequency response function, or transfer function, say $F(\omega)$. This function will exhibit waviness with sharp peaks at the resonant frequencies. As was pointed out by Lysmer (1974) in the course of a lecture on the interpolation of transfer functions, the inverses of such transfer functions behave locally as quadratic parabolas, and especially so in the neighborhood of the peaks. Thus, they behave locally as one degree-of freedom systems for the mode that is mainly active at that peak, i.e. $K(\omega) = F^{-1}(\omega) \sim k + i\omega c - \omega^2 m$, where, of course k, c, m depend on the frequency, but not too strongly if the modes are well separated. Since a parabola has only two derivatives, its Taylor series expansion has only two terms, so the expansion is exact no matter how large the perturbation. By contrast, this is not the case for the original transfer function $F(\omega)$, which tolerates only small perturbations, and then again only away from the resonant peaks.

Application to impedance functions via the DSE

As was shown earlier, a complex frequency is a form of damping, and as such it ameliorates or eliminates reverberations in the system being considered, a characteristic that is used in the DSE method to simulate an impedance function for an infinite domain by means of one of finite

extension, as will be shown next by means of canonical models in one, two and three dimensions.

Consider the stiffness or impedance function $K(\omega)$ for some elastodynamic problem, which depends on the excitation frequency and carries an implied exponential factor $\exp(\mathrm{i}\omega t)$. Instead of estimating the damped stiffness from the undamped one as explained earlier, we follow the example of Wolf and Song, and proceed to do the reverse process. For this purpose, we start from the trivial identity $K(\omega) \equiv K(\omega - \mathrm{i}\eta + \mathrm{i}\eta) = K(\varpi + \mathrm{i}\eta)$ and expand it in Taylor series:

$$K(\omega) = K(\varpi) + \mathrm{i}\eta\, K'(\varpi) - \tfrac{1}{2}\eta^2 K''(\varpi) + \cdots \tag{7a}$$

$$K'(\varpi) = \frac{\partial K(\varpi)}{\partial \varpi} = \frac{\partial K(\omega - \mathrm{i}\eta)}{\partial \omega} \tag{7b}$$

$$K''(\varpi) = \frac{\partial^2 K(\varpi)}{\partial \varpi^2} = \frac{\partial^2 K(\omega - \mathrm{i}\eta)}{\partial \omega^2} \tag{7c}$$

The equivalences in 7b, 7c follow because, as indicated earlier the derivatives of analytical functions do not depend on the direction they are taken. Hence, one can estimate the response for *real* frequency from that for *complex* frequency by means of the expression above. As will be seen later, the last term in the second derivative can (and should) be neglected in most cases.

Example 1: Finite vs. infinite rod (1-D)

Consider a rod of mass density ρ, Young's modulus E, cross-section A and length L. Without loss of generality, we assume that the rod is clamped at the right end and that a compressive harmonic force $Pe^{\mathrm{i}\omega t}$ is applied at the origin, which coincides with the left, free end. This rod can sustain waves that propagate with velocity $c = \sqrt{E/\rho}$. Solving the boundary value problem by standard methods, we obtain a relationship between the magnitude of the force and the displacement at the point where the load is applied u_0 of the form

$$P = \rho c \omega A \cot(kL)\, u(0,\omega) = K u_0, \qquad k = \omega / c \tag{8}$$

The term

$$K(\omega) = \rho c \omega A \cot(\omega L / c) \tag{9}$$

is the *real* impedance (dynamic stiffness) of the undamped rod as seen from the free end, which exhibits infinitely many singularities. In contrast, if we start with an infinite rod and replace the displacement boundary condition at $x = L$ by a radiation condition at $x = \infty$, we obtain instead

$$K^{\infty}(\omega) = \mathrm{i}\rho c \omega A \tag{10}$$

This is a *purely imaginary* impedance with no singularities, which can be interpreted physically as a viscous dashpot. In the light of these results, it would seem implausible at first that we could recover this function from the purely real, oscillating stiffness function of the finite rod, but that is precisely what we shall demonstrate next. Indeed, if in equation 9 we consider instead complex frequencies $\varpi = \omega - i\eta$, and use that expression to estimate the impedance for real frequencies by means of the Taylor series formula with only two terms, we obtain

$$\begin{aligned} K(\omega) &= K(\varpi + i\eta) \approx K(\varpi) + \mathrm{i}\eta K'(\varpi) \\ &= \rho c A\left\{\varpi \cot(\varpi L/c) + \mathrm{i}\eta\left[\cot \varpi L/c - \varpi L/c \sin^{-2}(\varpi L/c)\right]\right\} \\ &= \mathrm{i}\rho c A\left\{\frac{\omega}{\mathrm{i}}\cot\left(\frac{\varpi L}{c}\right) - \frac{\eta L}{c}\left(\frac{\varpi L}{c}\right)\sin^{-2}\left(\frac{\varpi L}{c}\right)\right\} \end{aligned} \tag{11}$$

If $T = L/c$ is the travel time of rod waves to the fixed boundary, and defining dimensionless variables $x = \omega T$ and $y = \eta T$, it is easy to show that when y is large, say $y > 4$, then $\tanh y \to 1$, $\cot(x - \mathrm{i}y) \to \mathrm{i}$, and $\sin^{-2}(x - iy) \to -4\exp(-2y)\exp(-2\mathrm{i}x)$. Hence

$$K(\omega) \approx \mathrm{i}\rho c A\left[\omega(1+\varepsilon) - \mathrm{i}\eta\varepsilon\right] \tag{12a}$$

$$\varepsilon = 4y\exp(-2\mathrm{i}x)\exp(-2y), \qquad x = \frac{\omega L}{c}, \qquad y = \frac{\eta L}{c} \tag{12b}$$

We see that $K(\omega) \to K^{\infty}(\omega)$ when $|\varepsilon| \to 0$, i.e. when $|\varepsilon| < 10^{-m}$, with m being an appropriate exponent, say 2 or 3. The smallest recommended value $y = \eta T = 4$ corresponds to $m = 2.17$ (i.e. an attenuation by about two order of magnitude). Observe that T decreases as Poisson's ratio increases because E and thus c increases. On the other hand, the static stiffness of the rod inferred from eq. 11 is

$$K(0) = K(-\mathrm{i}\eta) + \mathrm{i}\eta K'(-\mathrm{i}\eta) = \frac{EA}{L}\left[\frac{y}{\sinh y}\right]^2 \tag{13}$$

which for sufficiently large $y = \eta T$ is but a small fraction of the static stiffness EA/L of the finite rod, and tends rapidly to zero as y increases. Hence, we conclude that for sufficiently large imaginary frequency, $K(\omega) \approx K(\varpi) + \mathrm{i}\eta K'(\varpi) \to K^{\infty}(\omega)$, that is, the projection of the impedance of the finite rod by means of the Taylor series formula converges to the *exact* impedance of the infinite, undamped rod. As will be seen in the numerical evaluation that follows, this projected impedance works well to an excellent degree, including at small frequencies or even at zero frequency; this is remarkable when one considers that the static stiffness of the finite rod is not zero. The condition for this to be true is that $\eta T > 4$, with $T = L/c$ being the travel time of waves to the far boundary of the rod. Observe that what matters is the product ηT, and not the actual length of the rod, so even a very short rod should produce correct results for a sufficiently large imaginary frequency.

Numerical results:
At first we computed the ratio of the impedance of the finite rod, computed by the Taylor series formula, and the impedance of an infinite rod, with $\eta T = 10$ for a frequency range $0 \le \omega T \le 5$, which covers about 16 resonant modes of the finite rod. A value of 1 in this ratio is ideal, i.e. it would mean that the approximation matches *exactly* the infinite system. The agreement obtained with these simulation parameters was so good throughout the entire frequency range that the plot need not be shown here, for the graph would only have shown the exact solution. We then repeated the calculation with shorter lengths of the rod until we detected discrepancies from the ideal. These began to crop up when $\eta T < 5$ or so, i.e. in the vicinity of the limit $\eta T = 4$.

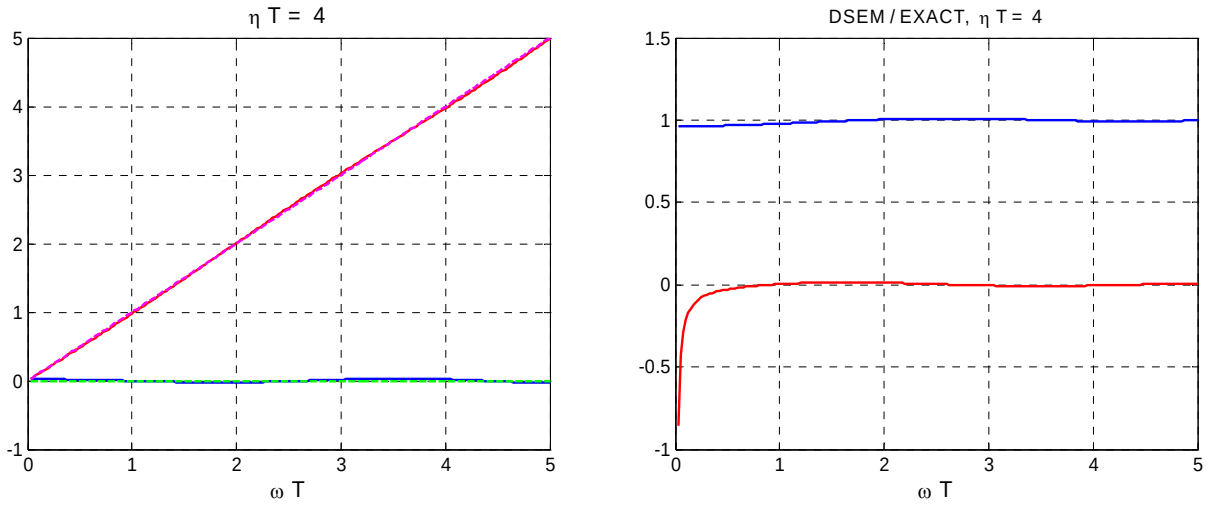

Figure 1: Finite rod vs. infinite rod. The left shows the real and imaginary parts of the impedance of the rods, while the right shows the ratio of the impedances.

Figure 1 on the left shows the impedance obtained by the extrapolation method with a finite rod vs. the exact impedance of an infinite rod when $\eta T = 4$. While there are four lines in this plot, namely two for the real part and two for the imaginary, these can hardly be distinguished from one another because the impedances are virtually identical, and this is verified in the figure on the right showing the ratio of the two impedances. The lower curve that hovers around zero is the imaginary part of this ratio, while the upper curve in the vicinity of 1 is the real part. As can be seen, the agreement is excellent indeed. Observe that the "perturbation" $\eta T = 4$ is gigantic, yet the projected impedance is still in remarkably good agreement with the impedance of the infinite medium. However, attempts to apply this method to a flexibility function with the large values of damping employed herein for the stiffness functions lead to gross failure.

Counter-example 2: Layered rod (1-D)
As a counter-example to the previous, very well-behaved problem, consider next a rod of finite length L_1 that is followed by another rod of infinite length $L_2 = \infty$ and different material properties. The goal here is to assess the DSE for a heterogeneous medium where waves may reverberate within the system even when the medium is infinitely long. This is simulated here by means of a *finite* rod consisting of two segments of arbitrary lengths and material properties, as

shown in the figure below. The right end is assumed to be fixed, and the harmonic load is applied at the left, free end.

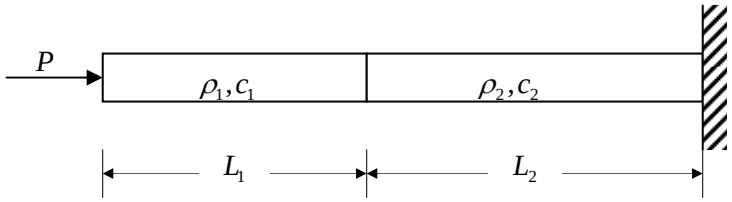

Figure 2: Rod with two material layers

Using standard methods in structural mechanics, it can be shown that the impedance of the composite, finite rod, as seen from the point of application of the external force, is

$$K = \rho_1 c_1 \omega \frac{\kappa - \tan\theta_1 \tan\theta_2}{\tan\theta_2 + \kappa \tan\theta_1}, \qquad \kappa = \frac{\rho_2 c_2}{\rho_1 c_1}, \qquad \theta_j = \frac{\omega L_j}{c_j} \tag{14}$$

Also, the impedance of an infinite rod (i.e. $L_2 = \infty$) is

$$K^{\inf} = \mathrm{i}\,\rho_1 c_1 \omega \frac{\kappa + \mathrm{i}\tan\theta_1}{1 + \mathrm{i}\kappa \tan\theta_1} \tag{15}$$

We observe that this impedance is either complex or purely imaginary, but never purely real. When purely imaginary, $K^{\inf} = \mathrm{i}\,\omega\rho_2 c_2$, which equals the impedance of a uniform rod, and this occurs at the resonant frequencies of the first segment as if it were free on both ends, i.e. $\omega_j = j\pi c_1 / L_1$.

The above equations were implemented into a Matlab script and tested at first with uniform material properties, the results of which were found to give results in perfect agreement with those in example 1. Figure 3 shows typical results for a non-uniform rod with $c_2 / c_1 = 2$, $L_2 / L_1 = 1$, travel time $T = L_1 / c_1 + L_2 / c_2 = 1$, and an imaginary frequency $\eta T = 4$. The results exhibit strong errors that persist even with much larger imaginary frequencies and no matter how long the second segment is made. Thus, the DSE method breaks down precipitously when the material properties are not uniform, a situation that was suspected to be true and motivated this counter-example. It should be mentioned that the discrepancies in this example could be reduced somewhat by adding material damping to the second rod. However, no combination of damping and imaginary frequency was found that could eliminate these errors, not to mention that the very addition of material damping actually invalidates the very principle on which the DSE rests. This finding strongly indicates that the DSE will fail to work in either two or three dimensions when the material is heterogeneous, for example a foundation embedded in layered media.

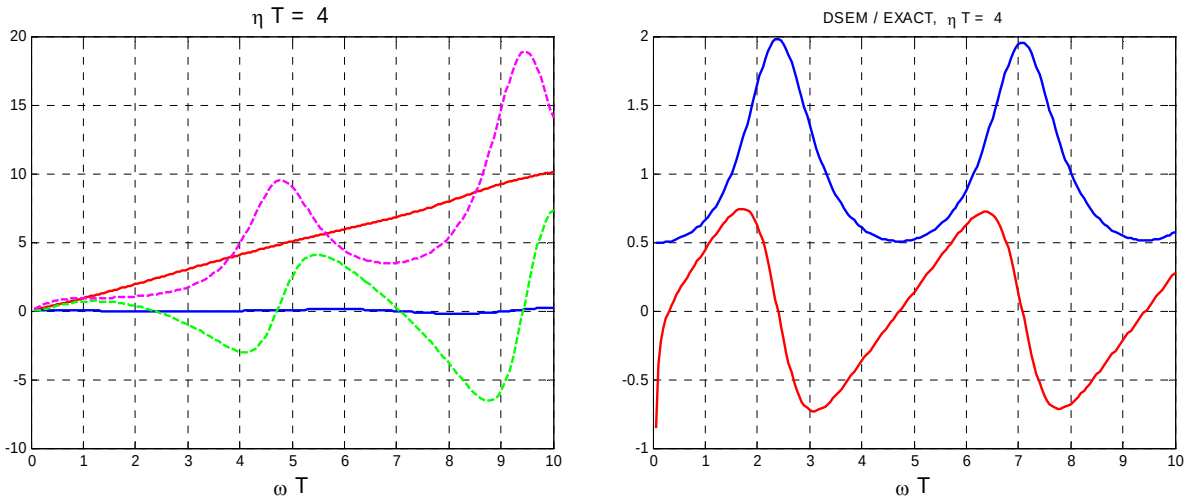

Figure 3: Layered rod with $c_2 / c_1 = 2$. The left shows the DSE vs. the actual impedance, while the right depicts the complex ratio of these two impedances.

Example 3: Translational stiffness of rigid cylinder (2-D)

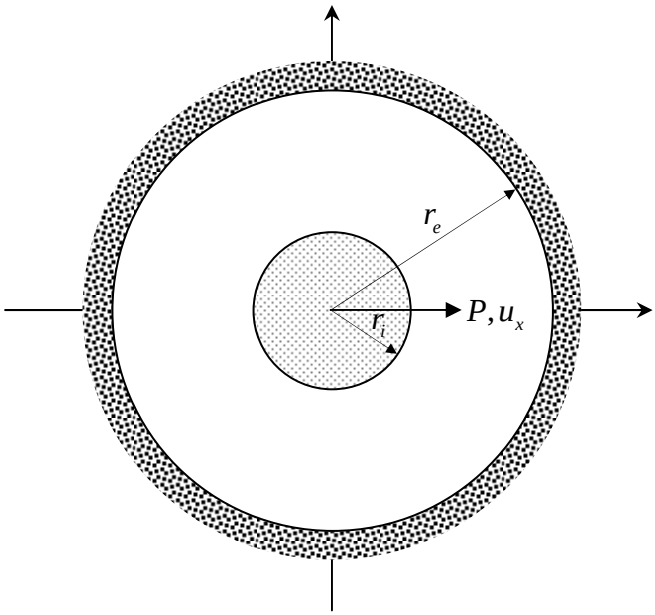

Figure 4: Rigid cylinder embedded in cylindrical annulus

Consider next a rigid, massless cylinder embedded in a homogenous two-dimensional space. The cylinder is subjected at its center (i.e. axis) to a harmonic force in some fixed radial direction, say the horizontal, which causes the cylinder to oscillate in that direction, and the ratio of the applied force to the observed oscillation is the lateral dynamic stiffness or impedance of the cylinder. This is conceptually similar to the problem of a semi-cylindrical foundation at the surface of an elastic half-space undergoing oscillations transverse to the free surface, but the latter is more

complicated because of the presence of that surface. To assess the performance of the DSE for this problem, we proceed to replace the infinite medium by a finite annular region with fixed external boundary, as shown schematically in Fig. 4.

It can be shown (Kausel, 2006) that the cylindrical displacement components at any arbitrary point and the stresses acting on cylindrical surfaces are of the form

$$\mathbf{u}(r,\theta,\omega) = \begin{Bmatrix} u_r \\ u_\theta \end{Bmatrix} = \mathbf{T}\left(\mathbf{H}_1 \mathbf{c}_1 + \mathbf{H}_2 \mathbf{c}_2\right) = \mathbf{T}\tilde{\mathbf{u}} \tag{16a}$$

$$\mathbf{s}(r,\theta,\omega) = \begin{Bmatrix} \sigma_{rr} \\ \sigma_{r\theta} \end{Bmatrix} = \tfrac{1}{r}\mathbf{T}\left(\mathbf{F}_1 \mathbf{c}_1 + \mathbf{F}_2 \mathbf{c}_2\right) = \mathbf{T}\tilde{\mathbf{s}} \tag{16b}$$

$$\mathbf{T} = \mathrm{diag}\begin{pmatrix} \cos\theta & -\sin\theta \end{pmatrix} \tag{16c}$$

in which $\mathbf{c}_1, \mathbf{c}_2$ are vectors of as yet arbitrary constants, $\mathbf{u}, \mathbf{s}$ are the actual displacements and stresses in cylindrical coordinates, $\tilde{\mathbf{u}}, \tilde{\mathbf{s}}$ contain the amplitudes of these quantities and $\mathbf{T}$ gives their variation in the azimuth. The elements of the matrices $\mathbf{H}_k$ and $\mathbf{F}_k$ are assembled with first and second Hankel functions of the radial position r, and these are listed in full in Table 1. In combination with an implied harmonic factor $\exp(\mathrm{i}\,\omega t)$, the terms in $\mathbf{H}_1$ represent waves that travel towards the axis, and those in $\mathbf{H}_2$ are waves that travel away from this axis. Hence, when the cylinder is embedded in an infinite space $r_e \to \infty$, the radiation condition demands $\mathbf{c}_1 = \mathbf{0}$, in which case $\tilde{\mathbf{u}}_i = \mathbf{H}_{i2}\mathbf{c}_2$ and $\tilde{\mathbf{s}}_i = \frac{1}{r_i}\mathbf{F}_{i2}\mathbf{c}_2$, where the added sub-index i identifies the inner cylindrical surface $r = r_i$ at which the Hankel functions are evaluated. The tractions per radian exerted by the rigid cylinder onto the soil at this inner interface are equal and opposite to the internal stresses at that location, times the radius of the inner surface, i.e. $\tilde{\mathbf{p}}_i = -r_i\,\tilde{\mathbf{s}}_i = -\mathbf{F}_{i2}\mathbf{c}_2$. Eliminating the constants of integration $\mathbf{c}_2$ between $\tilde{\mathbf{u}}_i$ and $\tilde{\mathbf{p}}_i$, we find $\tilde{\mathbf{p}}_i = \mathbf{K}^{\inf}\,\tilde{\mathbf{u}}_i$, where $\mathbf{K}^{\inf}$ is the impedance matrix for the infinitely large exterior region

$$\mathbf{K}^{\inf} = -\mathbf{F}_{i2}\mathbf{H}_{i2}^{-1} = \begin{Bmatrix} K_{11}^{\inf} & K_{12}^{\inf} \\ K_{21}^{\inf} & K_{22}^{\inf} \end{Bmatrix} \tag{17}$$

This matrix is symmetric and complex. By contrast, in the case of a finite annular region with a fixed external surface at radius r_e, the boundary condition $\mathbf{u}_e = \mathbf{0}$ demands $\mathbf{c}_1 = -\mathbf{H}_{e1}^{-1}\mathbf{H}_{e2}\,\mathbf{c}_2$, so the displacements and tractions per radian are now

$$\tilde{\mathbf{u}}_i = \left(\mathbf{H}_{i2} - \mathbf{H}_{i1}\mathbf{H}_{e1}^{-1}\mathbf{H}_{e2}\right)\mathbf{c}_2 \tag{18a}$$

$$\tilde{\mathbf{p}}_i = \left(\mathbf{F}_{i1}\mathbf{H}_{e1}^{-1}\mathbf{H}_{e2} - \mathbf{F}_{i2}\right)\mathbf{c}_2 \tag{18b}$$

Hence, the impedance matrix of the annular region, as seen from the interior is

$$\begin{aligned}\mathbf{K} &= \left(\mathbf{F}_{i1}\mathbf{H}_{e1}^{-1}\mathbf{H}_{e2} - \mathbf{F}_{i2}\right)\left(\mathbf{H}_{i2} - \mathbf{H}_{i1}\mathbf{H}_{e1}^{-1}\mathbf{H}_{e2}\right)^{-1} \\ &= \left(\mathbf{F}_{i1}\mathbf{H}_{e1}^{-1} - \mathbf{F}_{i2}\mathbf{H}_{e2}^{-1}\right)\left(\mathbf{H}_{i2}\mathbf{H}_{e2}^{-1} - \mathbf{H}_{i1}\mathbf{H}_{e1}^{-1}\right)^{-1} \\ &= \begin{Bmatrix} K_{11} & K_{12} \\ K_{21} & K_{22} \end{Bmatrix}\end{aligned} \tag{19}$$

Despite appearances to the contrary, this matrix is purely real, and it is also symmetric. (In principle, the first and second Hankel functions used here could be replaced with conventional Bessel and Neumann functions, but this is not convenient because the latter become quasi linearly dependent when their arguments are complex, a situation that leads to numerical difficulties). Now, when the cylinder undergoes rigid-body lateral displacements u_x, that implies displacement in cylindrical components at the inner surface of the form $\tilde{u}_{ri} = \tilde{u}_{\theta i} = u_x$. Hence, the actual tractions per radian at the inner surface are

$$p_r = \tilde{p}_r \cos\theta = \left[\left(K_{11} + K_{12}\right)u_x\right]\cos\theta \tag{20a}$$

$$p_\theta = -\tilde{p}_\theta \sin\theta = -\left[\left(K_{21} + K_{22}\right)u_x\right]\sin\theta \tag{20b}$$

The total force is then

$$\begin{aligned}P &= \int_0^{2\pi}\left[p_r\cos\theta - p_\theta\sin\theta\right]d\theta = \int_0^{2\pi}\left[\tilde{p}_r\cos^2\theta + \tilde{p}_\theta\sin^2\theta\right]d\theta \\ &= \pi\left(\tilde{p}_r + \tilde{p}_\theta\right) \\ &= \pi\left(K_{11} + K_{12} + K_{21} + K_{22}\right)u_x = K\,u_x\end{aligned} \tag{21}$$

so

$$K = \pi\left(K_{11} + K_{12} + K_{21} + K_{22}\right) \tag{22}$$

is the lateral impedance of the rigid cylinder embedded in a finite annular region with fixed outer boundary. Similarly,

$$K^{\inf} = \pi\left(K_{11}^{\inf} + K_{12}^{\inf} + K_{21}^{\inf} + K_{22}^{\inf}\right) \tag{23}$$

is the lateral impedance of the cylinder embedded in an infinite medium.

The lateral impedances $K, K^{\inf}$ and their derivatives with respect to frequency can be evaluated in closed-form by means of the symbolic tools in Matlab. However, the resulting formulas are too long and complicated to be reproduced herein.

TABLE 1

$$\Omega_S = \omega r / C_S , \qquad \Omega_P = \omega r / C_P = a\,\Omega_S , \qquad a = \frac{C_S}{C_P}$$

$$H_{nS}^{(k)} \equiv H_n^{(k)}\left(\Omega_S\right), \qquad H_{nP}^{(k)} \equiv H_n^{(k)}\left(\Omega_P\right)$$

$$\mathbf{H}_k = \begin{Bmatrix} H_{0P}^{(k)} - \frac{1}{\Omega_P} H_{1P}^{(k)} & \frac{1}{\Omega_S} H_{1S}^{(k)} \\ \frac{1}{\Omega_P} H_{1P}^{(k)} & H_{0S}^{(k)} - \frac{1}{\Omega_S} H_{1S}^{(k)} \end{Bmatrix}, \qquad k = 1, 2$$

$$\mathbf{F}_k = \begin{Bmatrix} f_{11}^{(k)} & f_{12}^{(k)} \\ f_{21}^{(k)} & f_{22}^{(k)} \end{Bmatrix}$$

$$f_{11}^{(k)} = -\left[\left(\lambda + 2G\right)\Omega_P H_{1P}^{(k)} + 2G\left(H_{0P}^{(k)} - \frac{2}{\Omega_P} H_{1P}^{(k)} \right) \right]$$

$$f_{12}^{(k)} = 2G\left(H_{0S}^{(k)} - \frac{2}{\Omega_S} H_{1S}^{(k)} \right)$$

$$f_{21}^{(k)} = 2G\left(H_{0P}^{(k)} - \frac{2}{\Omega_P} H_{1P}^{(k)} \right)$$

$$f_{22}^{(k)} = -G\left[\Omega_S H_{1S}^{(k)} + 2\left(H_{0S}^{(k)} - \frac{2}{\Omega_S} H_{1S}^{(k)} \right) \right]$$

Figure 5 shows the results of this formulation by varying the thickness ratio $\alpha = \left(r_e - r_i\right)/r_i$, Poisson's ratio ν and the imaginary component of frequency. The two sub-plots at the top show the results for $\nu = 0$ and a low value of the imaginary frequency. As expected, the results exhibit strong disagreements at all frequencies that persist even when the model is thick. The middle row of sub-plots show the results for the minimum recommended value $\eta T = 4$, and while the results are already good, a value ηT of five or six would have been better. Finally, the lower row of sub-plots is similar to the middle row, but evaluated at Poisson's ratio $\nu = \frac{1}{3}$. The plot on the left still shows important discrepancies that disappear as the model is made thicker. This demonstrates that the ideal value of the imaginary component of frequency should be chosen so that $\eta T_P \geq 4$, with T_P being the time of flight of P waves, which decreases with Poisson's ratio.

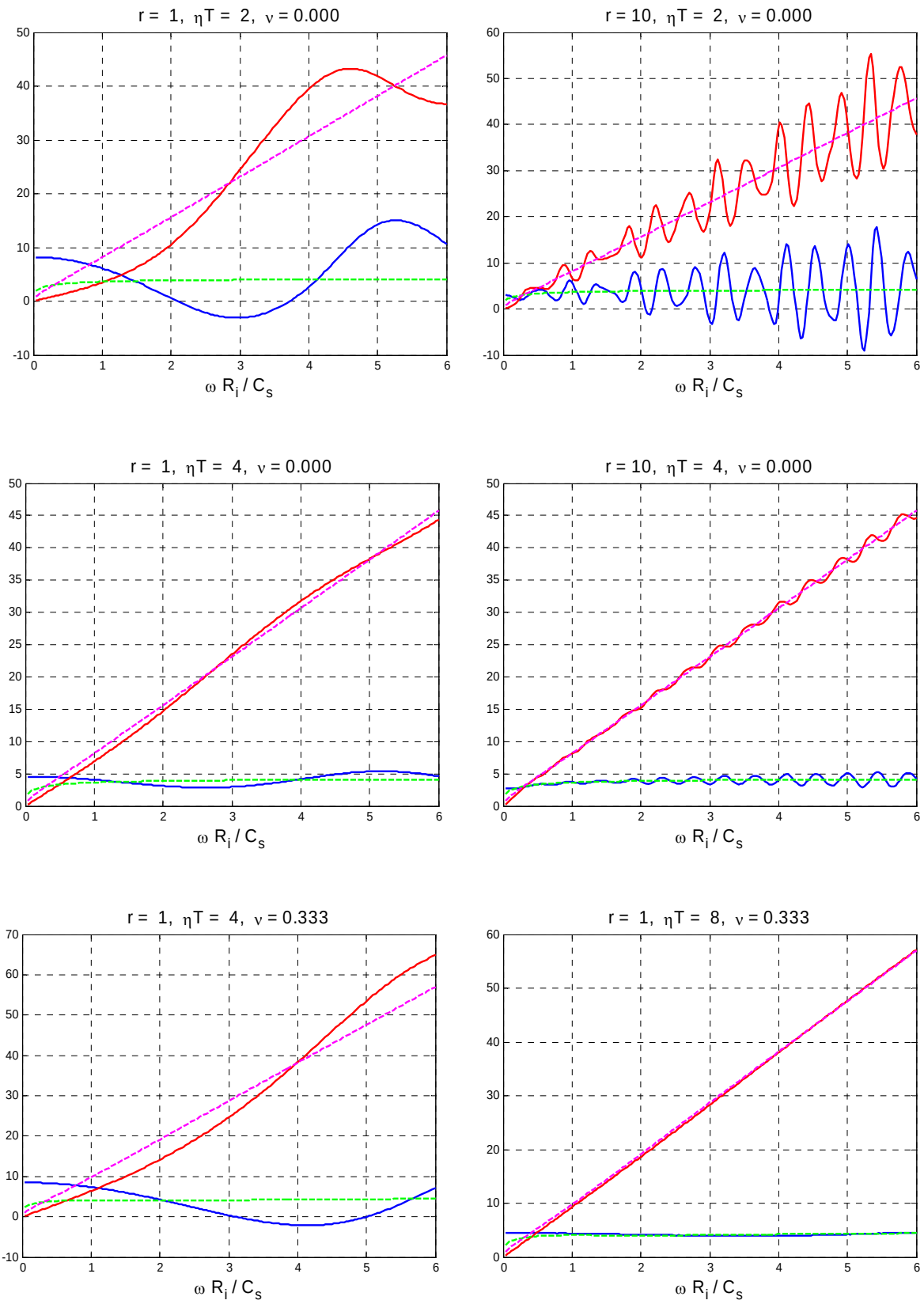

Figure 5: Rigid massless cylinder subjected to translation

Example 4: Massless, rigid sphere subjected to torsion (3-D)

Next, consider a hollow and massless, rigid sphere of radius R_i which is concentrically embedded in an elastic sphere of inner and outer radii R_i, R_e, mass density ρ, and shear modulus G. The rigid sphere is subjected to a torque. The outer spherical surface has some arbitrary boundary condition, which we take to be fixed. On its inner surface, the rigid sphere elicits time-harmonic azimuthal shearing tractions which are uniform in the azimuth but change with the sine of the polar angle (i.e. they attain a maximum at the equator and vanish at the poles). These tractions produce a total torsional moment M_t which causes pure shear waves to reverberate between the inner and outer surfaces, and they do so in such a way that at each radial distance from the center, the motion in spherical surfaces is like that of a rigid sphere. It can be shown that the torsional response of the sphere is governed by the following equations in spherical coordinates, e.g. see Kausel, 2006:

$$u\left(R,\phi,\theta\right) = \sin\phi\left(C_1\, h_1^{(1)} + C_2\, h_1^{(2)}\right) \tag{24}$$

$$\tau = G\left(\frac{\partial u}{\partial R} - \frac{u}{R}\right) = -G\,k\left(C_1\, h_2^{(1)} + C_2\, h_2^{(2)}\right)\sin\phi \tag{25}$$

in which R is the radial distance, ϕ is the polar angle (measured from the north pole), the $h_n^{(m)} = h_n^{(m)}\left(kR\right)$ are spherical Hankel functions of the m^{th} kind and n^{th} order, u is the tangential (azimuthal) displacement, and τ is the tangential stress. If the outer surface is fixed, then with the shorthand $h_{ne}^{(m)} = h_n^{(m)}\left(kR_e\right)$, we infer that $C_1\, h_{1e}^{(1)} + C_2\, h_{1e}^{(2)} = 0$ i.e. $C_2 = -C_1\, h_{1e}^{(1)} / h_{1e}^{(2)}$, which when substituted into the expression for the tangential stress and evaluating the result at the inner surface gives

$$\tau_i \equiv \tau\left(R_i,\phi,\theta\right) = G\,k\,C_1\left(\frac{h_{1e}^{(1)}}{h_{1e}^{(2)}}\, h_{2i}^{(2)} - h_{2i}^{(1)}\right)\sin\phi \tag{26}$$

The external tractions applied at the inner surface are equal and opposite to the internal stresses at that location, i.e. $p = -\tau$. These produce a net torsional moment

$$M_t = \int_0^{\pi}\int_0^{2\pi}\left(-\tau\right)R_i^3\sin^2\phi\; d\phi\, d\theta = \tfrac{8}{3}\pi G\, R_i^3\, k\, C_1\left(h_{2i}^{(1)} - \frac{h_{1e}^{(1)}}{h_{1e}^{(2)}}\, h_{2i}^{(2)}\right) \tag{27}$$

Also, the rotation of the inner surface equals the tangential displacement at the equator $\phi = \frac{1}{2}\pi$ divided by the radius, i.e.

$$\vartheta_i = \tfrac{1}{R_i}\left(C_1\, h_{1i}^{(1)} + C_2\, h_{1i}^{(2)}\right) = \tfrac{1}{R_i}C_1\left(h_{1i}^{(1)} - \frac{h_{1e}^{(1)}}{h_{1e}^{(2)}}\, h_{1i}^{(2)}\right) \tag{28}$$

Solving for the integration constant and substituting it into the expression for the torque, we obtain

$$M_t = \tfrac{8}{3}\pi G R_i^3 \frac{kR_i\left(h_{2i}^{(1)} h_{1e}^{(2)} - h_{1e}^{(1)} h_{2i}^{(2)}\right)}{h_{1i}^{(1)} h_{1e}^{(2)} - h_{1e}^{(1)} h_{1i}^{(2)}} \vartheta_i \tag{29}$$

The expression in front of ϑ_i is the torsional impedance of the hollow sphere as seen from the interior surface. Using the trigonometric representations of the spherical Hankel functions together with the definitions $z_e = kR_e$, $z_i = kR_i$ and after simplifications, the impedance function can be written as

$$K_t = 8\pi G R_i^3 \left\{1 + \tfrac{1}{3} z_i^2 \frac{z_e \cos\left(z_e - z_i\right) - \sin\left(z_e - z_i\right)}{\left(1 + z_i z_e\right)\sin\left(z_e - z_i\right) - \left(z_e - z_i\right)\cos\left(z_e - z_i\right)}\right\} \tag{30}$$

which in the absence of damping is purely real. The flexibility function is the inverse of the stiffness function, and the zeros of its denominator (i.e. the zeros of the stiffness' numerator) define the resonant torsional frequencies of the hollow sphere. The static stiffness (for $\eta = 0$) follows from the limit of K_t when $\omega \to 0$, an indeterminate form that is most conveniently obtained with Matlab's symbolic tool. The result is

$$K_0 = K_t\left(0\right) = 8\pi G \frac{R_i^3 R_e^3}{R_e^3 - R_i^3} \tag{31}$$

Finally, if the external radius is infinitely large and the external fixed boundary condition is replaced by a radiation condition, the moment-rotation equation reduces to

$$M_t = \tfrac{8}{3}\pi G R_i^3 \frac{z_i h_{2i}^{(2)}}{h_{1i}^{(2)}} \vartheta_i = 8\pi G R_i^3 \frac{1 + iz_i - \frac{1}{3} z_i^2}{1 + iz_i} \vartheta_i \tag{32}$$

that is,

$$K_t^{\infty} = 8\pi G R_i^3 \frac{1 + iz_i - \frac{1}{3} z_i^2}{1 + iz_i} \tag{33}$$

is the complex-valued torsional impedance of an infinite space as perceived by the spherical inclusion. Its static value is the factor in front of the fraction, which agrees with the static stiffness of the finite, hollow sphere when $R_e \to \infty$.

On the basis of the previous examples we assume that we can also estimate the torsional impedance of a spherical inclusion in an infinite space by means of the Taylor series formula

$$K\left(\omega, \alpha\right) \approx K\left(\omega - \mathrm{i}\eta, \alpha\right) + \mathrm{i}\eta K'\left(\omega - \mathrm{i}\eta, \alpha\right) - \tfrac{1}{2}\eta^2 K''\left(\omega - \mathrm{i}\eta, \alpha\right) \to K^{\infty}\left(\omega\right) \tag{34}$$

where $\alpha = \left(R_e - R_i\right)/R_i$ is the aspect ratio. As can be seen, unlike the rod that is characterized by just one dimensionless parameter, now we have two, namely $\eta T = \omega\left(R_e - R_i\right)/C_s$ and the aspect

(or thickness) ratio $\alpha = (R_e - R_i)/R_i$. Thus, merely choosing an appropriately large artificial damping, say $\eta T > 4$ may not be enough now because the results will depend on r as well.

The derivatives in 34 are rather messy, but can readily be evaluated with Matlab's symbolic tool. The result for the first derivative is

$$K_t' = \frac{dK_t}{d\omega} = \frac{K_0}{\omega}\frac{\frac{1}{3}z_i^2}{\Delta_1^2}\left\{\left[2(z_eC - S) + z_iC - z_e(z_e - z_i)S\right]\Delta_1 + (S - z_eC)\Delta_2\right\} \tag{35a}$$

$$C = \cos(z_e - z_i), \qquad S = \sin(z_e - z_i) \tag{35b}$$

$$\Delta_1 = (1 + z_iz_e)S - (z_e - z_i)C \tag{35c}$$

$$\Delta_2 = 2\,z_ez_i\,S + (z_e - z_i)(z_ez_iC + (z_e - z_i)S) \tag{35d}$$

The exact expression for the second derivative K_t'' can be also obtained with Matlab, but the final expression is too complicated to be reproduced here.

We have implemented these equations into a Matlab script and evaluated the DSE projection for various dimensionless parameters. Figure 6 shows a comparison of the impedances of the hollow sphere of finite thickness, projected with eq. 34 and using only the first derivative. The subplots on the left are for a thin sphere whose thickness equals the inner radius, and those on the right column are for a thick sphere with a thickness of four times the inner radius. In each case, the frequency on the horizontal axis is normalized by the inner radius, inasmuch as that is the parameter that controls the cavity in an infinite space. However, the imaginary component of frequency is normalized by the travel time of shear waves from the inner to the outer surface.

As can be seen, adding damping eliminates the waviness associated with the resonances in the sphere, and for $\eta T = 4$, the projected impedances are essentially those of the infinite space, except at low frequencies where some modest discrepancies are evident. From the last two plots at the bottom we also see that increasing the damping beyond this value does not help, but in fact makes matters worse.

Figure 7, on the other hand, shows the effect of adding the second derivative in eq. 34. One can see a rather small improvement at low frequencies and deterioration at higher frequencies. Numerical experiments with various other combinations of the parameters confirm this observation, which lead us to the conclusion that the derivatives higher than the first should be avoided. In fact, the "perturbation" which leads to optimal prediction is not small at all, but in fact enormous when contemplated in the context of a Taylor series.

Finally, when the thickness of the sphere, i.e. the size of the model, is increased to $r = 10$ and $\eta T = 4$ is used, the results were found to be virtually exact throughout the entire frequency range (hence, no figure need be shown).

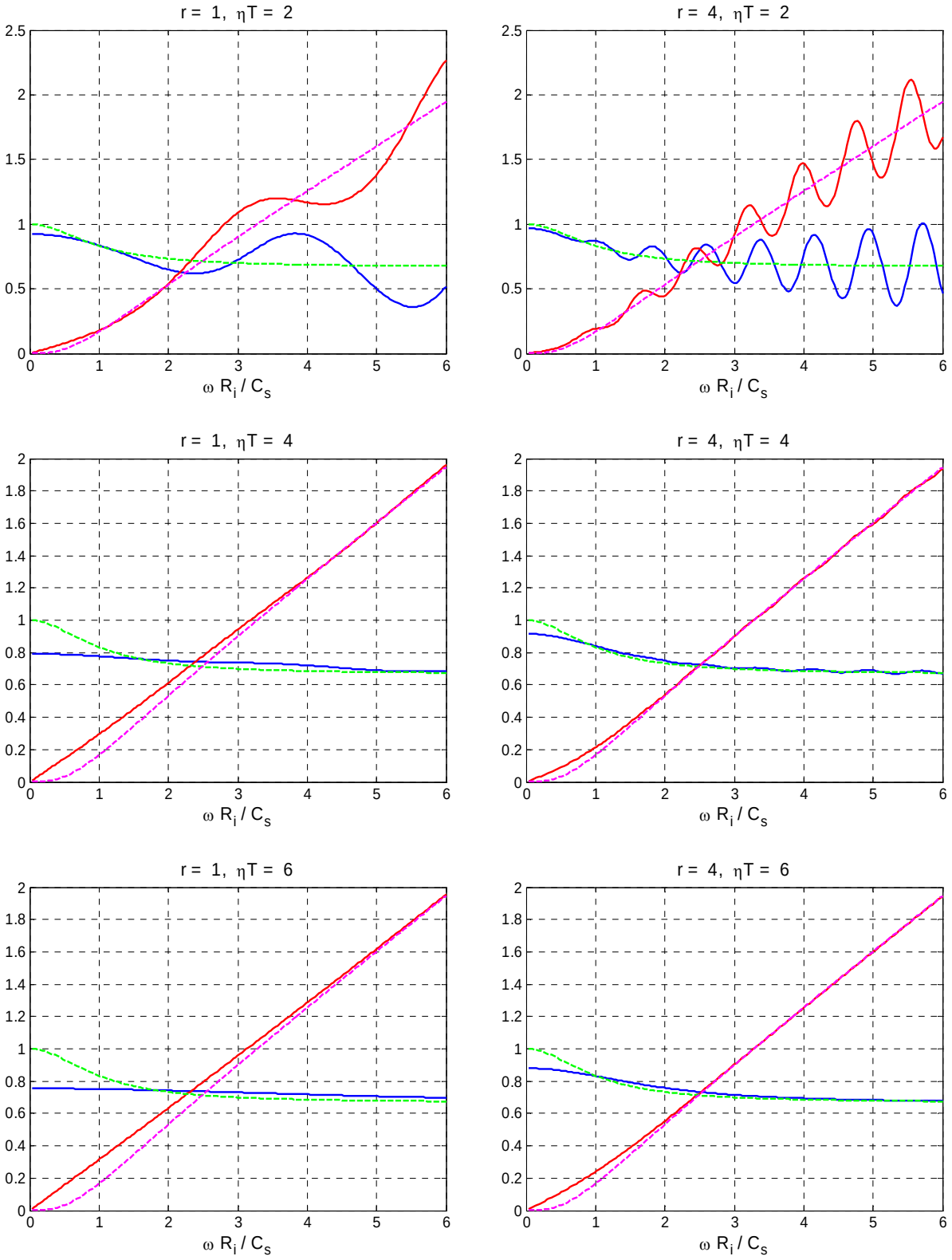

Figure 6: Torsional impedance of hollow sphere vs. spherical cavity in infinite space, with *r* = thickness of the sphere divided by inner radius.

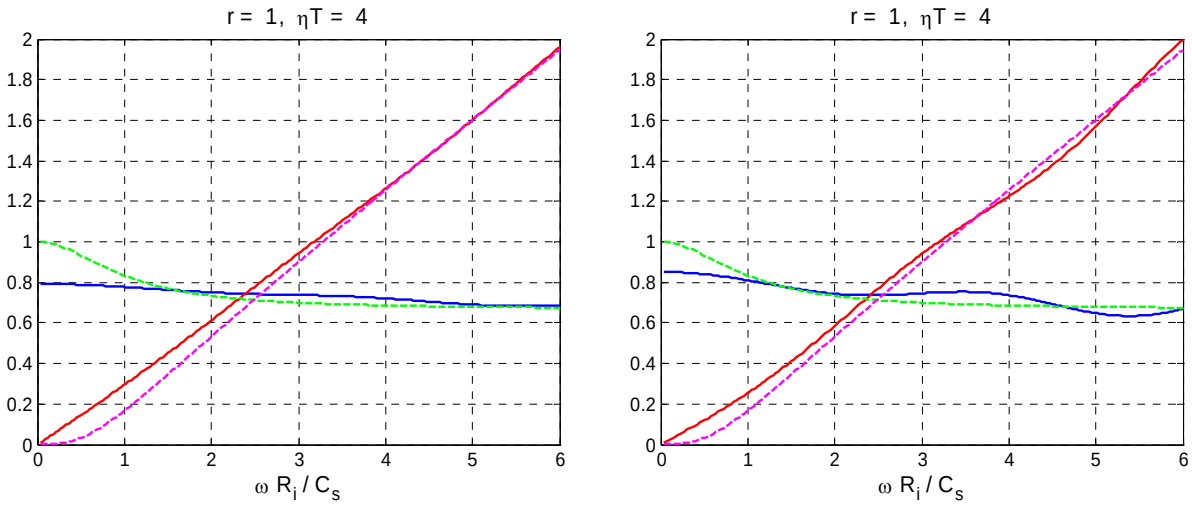

Figure 7: Effect of second derivative. Left = excluded, right = included

Example 5: Anti-plane (SH) transmitting boundary (2-D)

Finally, we consider a canonical problem involving arbitrarily many degrees of freedom, namely the impedance matrix, as seen from a fixed vertical section, of a system of homogeneous horizontal layers of infinite lateral extent which is subjected to SH sources. This corresponds very closely to the problem of a finite element mesh for a finite medium by means of which one seeks to obtain the dynamic stiffness of the infinite medium via the DSEM. This is perhaps the most remarkable canonical example examined herein, for it can be worked out in closed form from start to finish, no matter how many degrees of freedom the matrix may actually have.

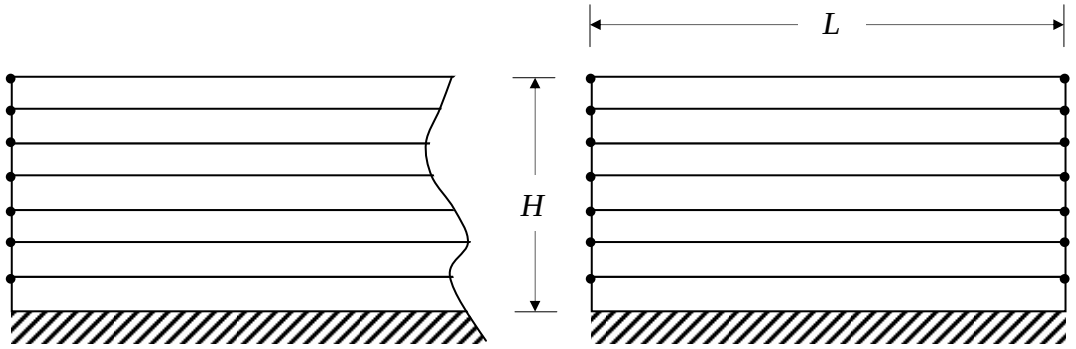

Figure 8: Semi-infinite stratum modeled with hyper-element of finite width

Consider a homogeneous stratum of depth H and infinite lateral extent that is modeled by means of the thin layer method (TLM), a procedure of the finite element type which consists in discretizing the system solely in the vertical direction. Thus, we subdivide this stratum into N layers that are thin in the finite element sense, see Fig. 8. The consistent transmitting boundary for this problem is known in closed form (Kausel & Tassoulas, 1981), and can be visualized as

the lateral impedance of the system of layers as if one had used infinitely many finite element columns. This boundary is highly accurate and absorbs *perfectly* not only all kind of waves, but also the evanescent displacement fields elicited by static loads.

TABLE 2: Definition of modal parameters

$\theta_{mn} = \frac{\pi}{2}\frac{(2m-1)(2n-1)}{2N+1}$,	$m,n = 1,2,\cdots N$	Modal angles
$\mathbf{\Phi} = \{\phi_{mn}\} = \{\cos\theta_{mn}\}$		Modal matrix
$\mathbf{\Phi}^T\mathbf{\Phi} = \frac{1}{4}(2N+1)\mathbf{I}$		Orthogonality condition
$\mathbf{\Phi}^{-1} = \frac{4}{2N+1}\mathbf{\Phi}^T$		Inverse of modal matrix
$\kappa_n = \sqrt{\left(\frac{\omega H}{C_s}\right)^2 - (2N+1)^2 \sin^2\left(\frac{\pi}{2}\frac{2n-1}{2N+1}\right)}$		Characteristic wavenumbers
$\mathbf{K} = diag\{\kappa_n\}$		Spectral matrix
$\mathbf{E} = diag\{\exp(-\mathrm{i}\kappa_n\lambda)\}$,	$\lambda = L/H$	Transport matrix

To simulate this problem with the DSE method, we model the stratum as a finite region of arbitrary width L, which we refer to as a hyper-element (or macro-element), and define the parameters given in Table 2 (the prefix "*diag*" identifies a diagonal matrix) . With these definitions, the infinite region can be shown to be characterized by the dynamic rigidity (i.e. impedance) matrix (Kausel and Tassoulas, 1981)

$$\mathbf{R}^{\inf} = \tfrac{1}{2}\mathrm{i}\,G\,\mathbf{\Phi}\mathbf{K}\mathbf{\Phi}^{-1} \tag{36}$$

On the other hand, the impedance matrix $\mathbf{R}$ for the stratum of finite width is (see Kausel & Roësset 1977, eqs.10a, 10b, adapted herein to the SH case)

$$\mathbf{R} = \begin{Bmatrix} \mathbf{R}_1 & \mathbf{R}_2 \\ \mathbf{R}_2^T & \mathbf{R}_1 \end{Bmatrix} = \begin{Bmatrix} \mathbf{R}^{\inf}\left[2\left(\mathbf{I}-\mathbf{J}^2\right)^{-1} - \mathbf{I}\right] & -2\mathbf{R}^{\inf}\mathbf{J} \\ symm & \mathbf{R}^{\inf}\left[2\left(\mathbf{I}-\mathbf{J}^2\right)^{-1} - \mathbf{I}\right] \end{Bmatrix} \tag{37a}$$

$$\mathbf{J} = \mathbf{\Phi}\mathbf{E}\mathbf{\Phi}^{-1} \tag{37b}$$

Observe that the dependence on frequency of the impedance matrix for the infinite region resides solely in the diagonal matrix $\mathbf{K}$. For the hyper-element as a whole, this dependence comes also through the cross-coupling matrix $\mathbf{J}$, which decreases in value as the width L increases because the characteristic wavenumbers have at least a small *negative* imaginary part due to material damping. However, when the frequency is made complex, the wavenumbers κ_n become strongly complex which cause in turn $\mathbf{E}$ and thus $\mathbf{J}$ to quickly tend to zero. This can be seen by examining the wavenumbers when the imaginary part of the frequency η is large and disregarding, just for illustration purposes, the second term in the square root. In that case,

$$\exp\left(-\mathrm{i}\,\kappa_n \lambda\right) \sim \exp\left(-\mathrm{i}\,\tfrac{\omega L}{C_S}\right)\exp\left(-\tfrac{\eta L}{C_S}\right) \to 0 \tag{38}$$

which means that for sufficiently large η, both $\mathbf{E} \to \mathbf{O}$ and $\mathbf{J} \to \mathbf{O}$ (the null matrix), implying that $\mathbf{R}_1(\varpi) \to \mathbf{R}^{\inf}(\varpi)$ and $\mathbf{R}_2(\varpi) \to \mathbf{O}$. Hence, on its left side, the hyper-element degenerates into a right-transmitting boundary, except that it is not quite what is desired because it is evaluated at a strongly complex frequency. The question is then whether or not $\mathbf{R}^{\inf}(\omega)$ can be recovered from $\mathbf{R}^{\inf}(\varpi)$ by means of a Taylor series expansion. Now, the derivatives with respect to frequency depend on the derivative of the characteristic wavenumbers, which is $\frac{d}{d\omega}\mathbf{K} = \omega\left(H / C_S\right)^2 \mathbf{K}^{-1}$. Designating as $\mathbf{K}_c = \mathbf{K}(\varpi)$, we have then

$$\tfrac{d}{d\omega}\mathbf{R}^{\inf}(\varpi) = \tfrac{1}{2}\mathrm{i}\,\varpi\, G\left(\tfrac{H}{C_S}\right)^2 \mathbf{\Phi}\mathbf{K}_c^{-1}\mathbf{\Phi}^{-1} \tag{39}$$

$$\begin{aligned}\hat{\mathbf{R}} &= \mathbf{R}^{\inf}(\varpi) + \mathrm{i}\,\eta\,\tfrac{d}{d\omega}\mathbf{R}^{\inf}(\varpi) \\ &= \tfrac{1}{2}\mathrm{i}\,G\,\mathbf{\Phi}\mathbf{K}_c\,\mathbf{\Phi}^{-1} + \mathrm{i}\,\eta\left[\tfrac{1}{2}\mathrm{i}(\omega - \mathrm{i}\,\eta)G\left(\tfrac{H}{C_S}\right)^2 \mathbf{\Phi}\mathbf{K}_c^{-1}\mathbf{\Phi}^{-1}\right] \\ &= \tfrac{1}{2}\mathrm{i}\,G\mathbf{\Phi}\left[\mathbf{K}_c + \mathrm{i}\,\eta(\omega - \mathrm{i}\,\eta)\left(\tfrac{H}{C_S}\right)^2 \mathbf{K}_c^{-1}\right]\mathbf{\Phi}^{-1} = \tfrac{1}{2}\mathrm{i}\,G\mathbf{\Phi}\hat{\mathbf{K}}\,\mathbf{\Phi}^{-1}\end{aligned} \tag{40}$$

We see that for $\hat{\mathbf{R}}$ to converge to $\mathbf{R}^{\inf}(\omega)$, it would be necessary that

$$\hat{\mathbf{K}} = diag\left\{\hat{\kappa}_n\right\} = \mathbf{K}_c + \mathrm{i}\,\eta(\omega - \mathrm{i}\,\eta)\left(\tfrac{H}{C_S}\right)^2 \mathbf{K}_c^{-1} \overset{?}{\to} \mathbf{K} \tag{41}$$

The above test of convergence can be written explicitly in terms of the modal wavenumbers as

$$\Delta = \frac{\hat{\kappa}_n - \kappa_n}{\omega_n} = \frac{(\omega - \mathrm{i}\,\eta)\,\omega / \omega_n^2 - 1}{\sqrt{(\omega - \mathrm{i}\,\eta)^2 / \omega_n^2 - 1}} - \sqrt{(\omega / \omega_n) - 1} \overset{?}{\to} 0 \tag{42}$$

with

$$\omega_n = \frac{C_S}{H}(2N+1)\sin\left(\tfrac{\pi}{2}\,\tfrac{2n-1}{2N+1}\right) \approx \frac{\pi C_S}{2H}(2n-1) \tag{43}$$

being the cutoff frequency of the n^{th} mode. To assess the quality of the above approximation, it suffices then to examine the dimensionless difference

$$\Delta = \frac{x(x-\mathrm{i}y)-1}{\sqrt{(x-\mathrm{i}y)^2-1}} - \sqrt{x^2-1} \overset{?}{\to} 0 \tag{44}$$

for a range of values of $x = \omega / \omega_n$ and $y = \eta / \omega_n$ (Note: the imaginary part of the term being subtracted should be negative when purely imaginary).

Figure 9 depicts this difference in the range $x = 0{:}10$ for $y = 0.25, 0.50, \cdots 1.25$. The sub-plot on the left is without damping, while the one on the right it has 2.5% material damping. In general, the error is largest at the cutoff frequency of the mode, and decreases rapidly above it. It also decreases in tandem with the imaginary component of frequency and if the soil has some material damping (which is especially effective in decreasing the error at the cutoff frequency $x = 1$). Still, to be useful, η must be large enough for the coupling matrix $\mathbf{J}$ to be negligible, a goal that can be achieved by making the width L appropriately large in comparison to the depth H. If $T = L / C_S$ is the travel time of shear waves across the width of the hyper-element, an error avoidance criterion would be then $\eta T \geq 4$ (which effectively makes $\mathbf{J}$ negligible), and $y = \eta / \omega_n \leq \frac{1}{2}$ (which causes $\hat{\kappa}_n \approx \kappa_n$). The latter condition is satisfied by all modes if it is satisfied by the first mode, i.e. if $\eta \leq \frac{\pi}{4} C_S / H$, and both criteria will be satisfied simultaneously if $L > \frac{16}{\pi} H \sim 5H$.

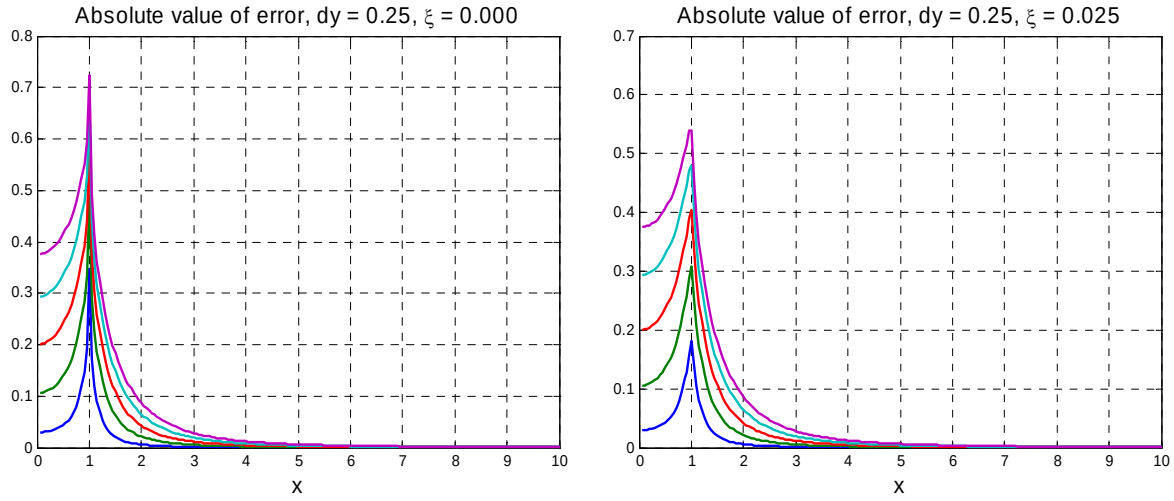

Figure 9: Error in modal wavenumber as function of frequency for 0% and 2.5% material damping.

This example suggests that it should be possible to use the DSE method to determine the impedance matrices for external, unbounded homogeneous regions, that is, to come up with effective transmitting boundaries of any shape. The requirement would be that the shortest

distance to the external boundary (the right boundary in this example) be some four or five times the largest width (here the depth) of the transmitting boundary, and that the product of the imaginary component of frequency and the shortest time of flight of waves to the outer boundary be on the order of four or more.

Conclusions

The DSE method allows computing the impedances associated with an infinite medium by means of a finite medium together with complex frequencies and extrapolating the results with the Taylor series formula. Rather remarkable is the fact that the procedure works at all, for the perturbations in damping required for this procedure to be useful are huge. From the numerical results for the canonical problems considered herein one can arrive at the following conclusions:

1) For the DSE to work satisfactorily, the level of artificial damping must be large, but within limits, for excessive values will lead to error. The recommended value is an imaginary frequency η such that the product of this frequency times the travel time of the fastest waves to the exterior boundary is approximately $\eta T = 4$ or so. This should work in one, two or three dimensions.

2) The DSE fails for inhomogeneous media, such as layered soils when the model is truncated in the direction of inhomogeneity (i.e. of layering). However, this does not affect truncation parallel to layering, for there are no material transitions in that direction.

3) The size of the model is relevant. The distance from the inner to the outer boundaries should be some four (or more) times the characteristic length of the region (e.g. largest dimension of the foundation, or the length of the transmitting boundary). In one dimension, this requirement is irrelevant.

3) The boundary conditions at the far end are irrelevant when the previous criteria are satisfied. There is in fact no need to complicate the model with coarse transmitting boundaries that may actually complicate the formulation and deteriorate the solution (and they may not help much in reducing the size of the numerical model anyway).

4) Attention must be paid to the size of the finite elements used. Elements that get more elongated as they approach the outer boundary may produce undesirable reflections, because the impedance contrast at the junction of dissimilar elements causes reflections that damage the capacity of the system to radiate. Also, the usual criterion of four to eight elements per wavelength may not be adequate for capturing the strongly evanescent wave fields elicited by the large imaginary parts being proposed herein, which cause the wave field to decay by some two orders of magnitude over comparatively short distances.

5) The canonical models presented in this paper were free of material damping, but such damping could readily be introduced by making the elastic moduli complex. However, its effect is rather small in comparison to that of the artificial damping achieved with complex frequencies, and thus it would not help in reducing the size of the finite element model. Hence, it is best left out.

6) The DSE works remarkably well for impedance functions, but fails miserably for flexibility functions, i.e. for frequency response functions. The latter can, of course, still be obtained by inversion of the stiffness functions.

7) The last example suggests that the DSE method could be used to obtain a transmitting boundary of arbitrary shape to simulate an infinite, homogenous exterior region. In the frequency domain, it would suffice to consider an exterior buffer layer (or region) with homogenous material properties, model it with finite elements and imaginary frequency components, condense out the outer degrees of freedom while maintaining the inner degrees of freedom, and use the projected impedance matrix as external boundary to the actual finite element model being analyzed. However, the size required for such a model could be large if the "radius" of the transition region is large on account of being an outer buffer layer.

References

1. Basu, U. and Chopra, A.K. (2002), "Numerical evaluation of the damping-solvent extraction method in the frequency domain", *Earthquake Engineering and Structural Dynamics*, **31**, 1231-1250.

2. Hall, J. and Beck, J.L. (1993), Linear system response by DFT: Analysis of recent modified method, *Earthquake Engineering and Structural Dynamics*, **22**, 599-615

3. Kausel, E. and Roësset, J.M. (1977), Semi-analytic hyper-element for layered strata, *Journal of the Engineering Mechanics Division*, ASCE, Vol. 103, EM4

4. Kausel, E. and Tassoulas, J.L. (1981), Transmitting boundaries: a closed form comparison, *Bulletin of the Seismological Society of America*, Vol 71, No 1, pp 143-159, February 1981

5. Kausel, E. and Roësset, J.M. (1992), "Frequency domain analysis of undamped systems", *Journal of Engineering Mechanics*, ASCE, **118** (4), 721-734.

6. Kausel, E. (2006), *Fundamental Solutions in Elastodynamics*, Cambridge University Press, Cambridge, England

7. Lysmer, J (1974), Lecture notes of a course on soil-structure interaction conducted at the University of California in Berkeley.

8. Phinney, R. A. (1965), "Theoretical calculation of the spectrum of first arrivals in a layered medium", *Journal of Geophysical Research*, **70**, 5107-5123.

9. Wolf, J.P. and Song, C. (1996), *Finite Element Modeling of Unbounded Media*, Wiley: Chichester, England